energies

MDPI

Article

Study on the Extensibility of Voltage-Plateau-Based Lithium Plating Detection for Electric Vehicles

Nithin Somasundaran *, Nessa Fereshteh Saniee, Truong Quang Dinh * and James Marco

Warwick Manufacturing Group (WMG), University of Warwick, Coventry CV4 7AL, UK
* Correspondence: nithin.somasundaran@warwick.ac.uk (N.S.); t.dinh@warwick.ac.uk (T.Q.D.); Tel.: +44-7760857606 (N.S.)

Abstract: Lithium plating is an undesirable side reaction in lithium-ion cells during fast charging at lower temperatures. The voltage plateau of the open-circuit voltage (OCV) of cells after charging is widely used to infer the onset of lithium plating. The differential analysis of post-charge OCV has been shown to yield greater insights into the Li stripping characteristics. Though this method is continuously evaluated for single cells in open circuit, a battery module can have a series and parallel connection of cells. The effectiveness and scalability of the voltage-plateau-based technique for battery modules is presented here. The study focuses on individual cells in open circuit, cells in parallel connection, and cells in a series-parallel connection. The results validate the scalability of the technique, yet the reliability and sensitivity were observed to be inferior to the single cell results published previously.

Keywords: lithium plating; voltage plateau; battery management system

Citation: Somasundaran, N.; Fereshteh Saniee, N.; Dinh, T.Q.; Marco, J. Study on the Extensibility of Voltage-Plateau-Based Lithium Plating Detection for Electric Vehicles. *Energies* **2023**, *16*, 2537. https://doi.org/10.3390/en16062537

Academic Editor: Carlos Miguel Costa

Received: 19 January 2023
Revised: 24 February 2023
Accepted: 26 February 2023
Published: 8 March 2023

1. Introduction

Electric vehicles (EV) employing lithium-ion batteries have gained huge popularity over the years. However, the range anxiety and long charging time have hindered EVs' extensive public acceptance [1,2]. To address these concerns, manufacturers often depend on energy dense cells and their fast-charging (FC) strategies. FC targets differ between manufacturers; however, many wish to charge the battery from 20 to 80% capacity [3] within 1 h. Li-ion batteries, when charged at a faster rate, have significant drawbacks [2]. One such aspect is the onset of undesirable side reactions, which leads to metallic lithium plating (LP) [4] on the graphite anode. LP is largely connected to FC and is aggravated at low operating temperatures [5]. At low temperatures and FC, the reduced charge kinetics lowers the anode potential less than the Li^+ reference and favors Li ions to be deposited as metallic lithium on the surface of the anode [6,7]. The contiguous plating and intercalation potential of graphite anodes make them prone to LP.

The effect of LP on the safety and cycle life of a cell is known to be significant, as LP in dendrite formation [7] can pierce through the separator and cause an internal short circuit [8]. Furthermore, metallic lithium deposits can isolate from further chemical reactions and lead to loss of lithium inventory (LLI) and energy and capacity fade [6]. Hence, the detection and prevention of LP during FC is deemed to be crucial. Metallic Li plated on the graphite anode can be subdivided as reversible and irreversible. The irreversible part of LP detaches from the anode and interacts with the electrolyte and contributes to LLI, whereas the reversible part undergoes further reactions and re-intercalates into the anode. This metallic lithium stripping and re-intercalation of reversible Li produces a voltage plateau in the open-circuit voltage (OCV) during the relaxation phase after a charging event [9]. The time differential of the voltage plateau of OCV ($\partial V/\partial t$), generally referred to as the voltage relaxation profile (VRP), can be used to estimate the Li stripping time [10] and, in turn, be employed as a proxy-metric to quantify the volume of reversible

LP [11]. There exist several other means of LP detection [12]; however, the majority of them such as (a) reference electrode, (b) neutron diffraction, (c) measurement of cell thickness, and (d) accurate coulombic efficiency, etc., require sophisticated equipment and test environments [9].

VRP, being a non-invasive and an easy-to-use technique, is widely used by researchers to develop and compare new FC charging strategies [13–15] that are appropriate for deployment within a battery management system (BMS). However, most of the existing literature focuses on cell-level analysis within a laboratory and the scalability of VRP to cells in series-parallel combinations has not been widely considered. Furthermore, VRP is defined and evaluated for cells in open circuit after charging. There are few reported studies on improving the detection capability of VRPs. U. Rao Koleti et al. [10] indicated that the current limits set during the constant voltage (CV) phase at the end of a constant current charge period greatly influence the detection capability. This is due to the initiation of Li stripping in the CV phase itself and demonstrated the increase in LP detection capability with a higher CV cut-off. However, this study was also limited to single cells.

Within an EV battery pack, generally there will be a parallel combination of cells that make up modules and subsequent modules connected in series to form the pack. The complex electrical connection within a battery pack will induce stray inductance. In addition to this, the cells in a pack will have current imbalance and cell-to-cell current flow existing even after charging [16], which invalidates the ideal open-circuit requirement for the VRP. The only reported literature on VRP that considered cells in parallel is by the authors of this article in [17].

Considering these factors, the study presented in this article aims to gain insight into the effectiveness of VRPs for inferring the onset of LP when cells are connected in series-parallel combination as part of a module. The preliminary research conducted in [17] is further extended, analyzed in detail, and presented here. The focus here is on the scalability of VRP; improving the LP detection sensitivity is not considered.

The article is structured as follows: Section 2 explains the experimental set-up and details of the tests performed on individual cells, cells in parallel, and cells in series parallel. Section 3 presents the test results and analysis. Finally, Sections 4 and 5 present the further work and conclusions from this study.

2. Experimental Details

LP is known to be highly influenced by ambient operating temperature [8], and hence, it is important to validate the tests at different temperatures. The temperatures considered for the study are 25, 10, 5, and 0 °C inside an ESPEC environmental chamber. The charging rates (C_{rates}) used were 0.3, 0.5, and 1C. The electrochemical performance of the cells was benchmarked with a reference test (defined in Section 2.2) at the beginning, over the course of the experiment, and at the end. The overall experimental process is depicted in Figure 1 and the experimental platform in Figure 2. The setup and VRP evaluation of cells in various scenarios are presented below.

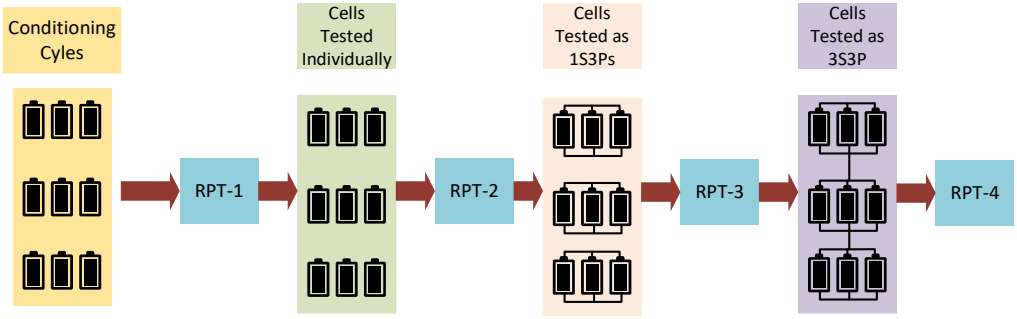

Figure 1. Experiment stages.

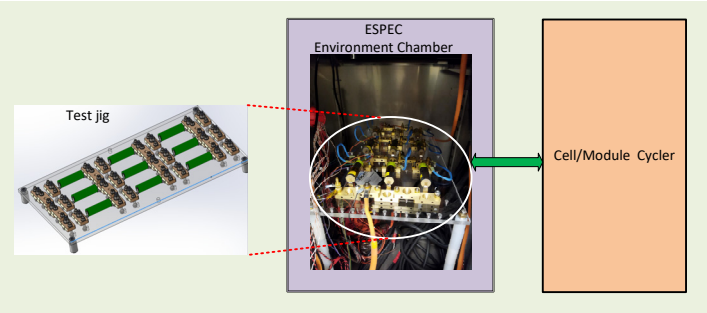

Figure 2. Experimental platform.

2.1. Cell Preparation

Commercially available INR21700 cells with a rated capacity of 4.8 Ah were used for the study. These cells have NCA chemistry with a graphite anode and the rated voltage is 4.2 V. The manufacturer's recommended charging strategy is constant current (CC) up to 4.2 V, followed by constant voltage (CV) with a cut-off of 0.05C. The C_{rate} of 1C is 4.8 A. Similarly, the discharging protocol is CC mode till 2.5 V. Nine cells of similar mass and internal resistance were selected for the experiment. The cells are labelled from 1 to 9 in order. The resistance was measured when cells were fully discharged at 25 °C using a HIOKI-BT3563 at 1kHz. The average resistance of the cells was around 16 mΩ.

2.2. Reference Performance Test

A detailed description of the reference performance test (RPT) process is defined in [18] but is included here for completeness. The RPT involves discharge capacity measurements and resistance measurements at different SoCs using discharge pulses. Cells are connected individually to 9 channels of a Maccor 4209 multirange cycler for RPT and kept inside an environmental chamber at 25 °C.

Cells are temperature soaked and adequately rested to stabilize before and after each step in the process. The rest periods were 2 h before and after a full charge and discharge for capacity measurement. The charging and discharging limits are the same as highlighted in Section 2.1. Discharge capacity is measured for 0.3C in CC mode till 2.5 V. For discharge pulses and SoC adjustments, the rest period considered is 1 h, which is the same as that employed in [18]. The discharge pulse used for resistance measurement is 0.5C, and the SoCs considered for measurements are 100, 80, 50, and 30%. SoC adjustments were performed with a 0.3C discharge in CC mode. Four RPTs were performed over the course of this study, and they are labelled as RPT-1 to 4.

2.3. Individual Cell Test for VRP

The unused cells were cycled three times before the actual tests to facilitate conditioning. The protocol followed was 0.3C CC mode till 4.2 V and CV with a 0.05C limit, and the discharge was 0.3C in CC with 2.5 V as the lower limit. The cells, after conditioning cycles, underwent an RPT. The average cell capacity from RPT-1 was 4.66 Ah and resistances were 16.17 and 16.35 mΩ at 100 and 30% SoC, respectively.

The cells were mounted on a customized Perspex jig with brass connectors, placed inside an ESPEC chamber, and wired to a Maccor cycler. The cells were charged in CC-CV mode at rates of 0.3, 0.5, and 1C for 3 cycles under temperatures of 25, 10, 5, and 0 °C. Afterwards, cells were rested with no electrical load for a duration of 4 h to achieve electrical equilibrium. The OCV during rest was recorded by the Maccor cycler at an interval of 1s. The VRP was computed from the rest period OCV. The VRP of individual cells and analysis is given in Section 3.1.

2.4. Scaling to 1-Series and 3-Parallel (1S3P) Configuration

The cells after individual tests for VRP were discharged and subjected to RPT-2. The average internal resistance increased by 1.22% and capacity reduced by 2.12% from the initial value. It is assumed that this is mainly due to accelerated ageing associated with LP. However, the changes in capacity and resistance were uniform across all the cells.

The cells after RPT were discharged completely and formed into parallel modules of three. Three 1S3P modules were made with the help of brass blocks connected on the negative terminal and a 6mm^2 copper cable of 20 cm length having 0.9 mΩ resistance on the positive side. The reason for using cables at the positive terminal is to facilitate the inclusion of an additional clamp-on current sensor connection. Cells 1, 2, and 3 formed the first 1S3P; 4, 5, and 6 formed the second; and 7, 8, and 9 were connected as the third 1S3P.

Two Tektronix TCP312A current probes (CT) were used with TCPA300 amplifiers for each 1S3P; the output of these were interfaced to a Pico Log ADC-24 data acquisition system interfaced to a laptop for data recording at a rate of 1Hz. The sensors are capable of accurately measuring currents with a sensitivity of $\pm$1 mA. The circuit and connections of the 1S3P modules are shown in Figure 3. The currents of Cell 3, Cell 6, and Cell 9 were computed based on Kirchhoff's current law (KCL), considering the current recorded by the Maccor cycler for respective modules.

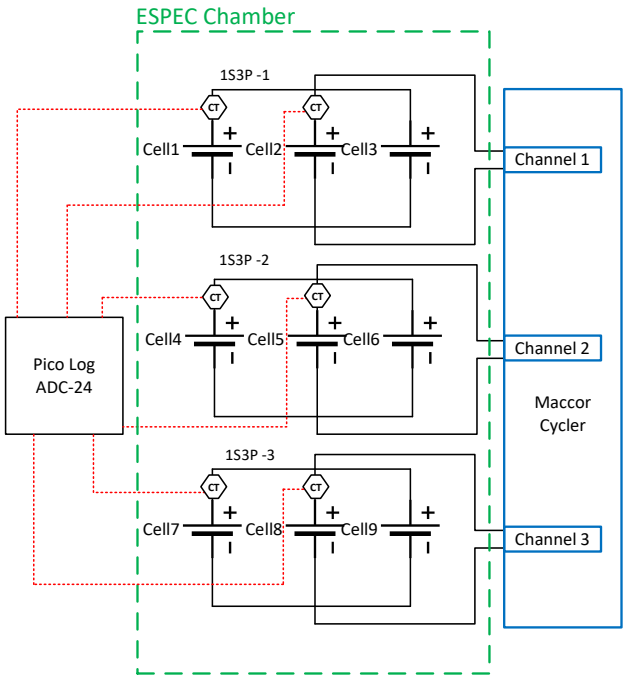

Figure 3. Schematic and connection of cells in 1S3P module.

2.5. Scaling to 3-Series and 3-Parallel (3S3P) Configuration

The cells in 1S3Ps were disconnected and RPT-3 was performed. Later, the cells were connected to form the 3S3P module, as seen in Figure 4. Rows 1, 2, and 3 represent each of the 1S3Ps within the 3S3P system, respectively. The 3S3P module was placed in an ESPEC chamber and was wired to a Chroma 17020 module cycler. The currents of Cell 3, Cell 6, and Cell 9 were computed based on KCL, considering the current recorded by the Chroma cycler for the module.

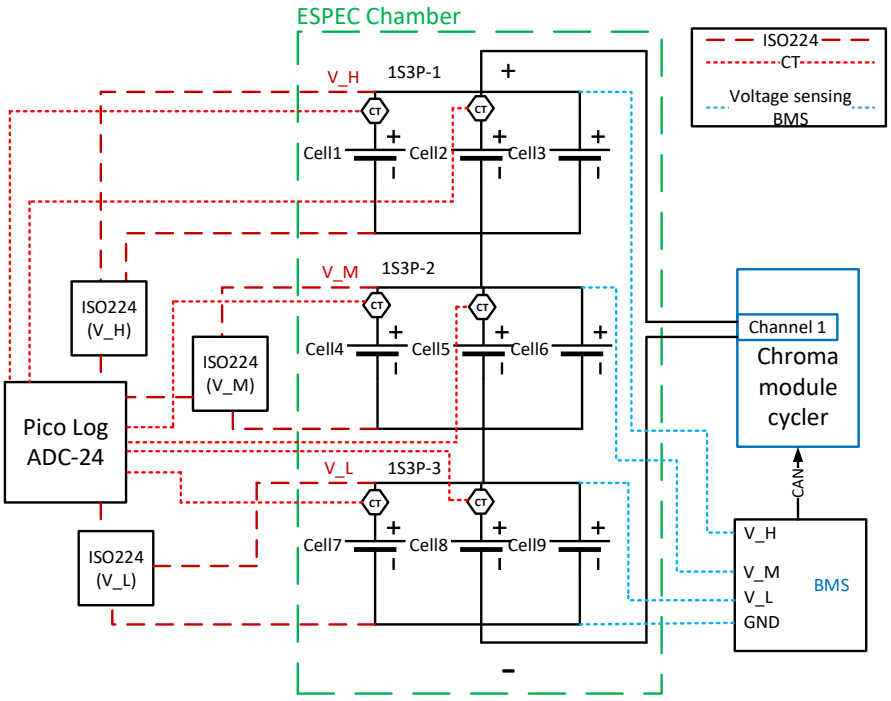

Figure 4. Schematic and connections of 3S3P module.

To prevent over charging and over discharging of cells, a generic BMS (Orion Jr 2) was used. The BMS was configured according to the module specifications and was set to transmit the lowest cell voltage and highest cell voltage data measured in the module. Additional ISO224 precision voltage sensing isolation amplifiers were used to measure the voltages of each row in the 3S3P. The output from the voltage sensors was interfaced to PicoLog ADC-24. The isolation amplifier prevents short circuit of cell negative terminals via the ground pin of ADC-24 and thus ensures the safety of cells and measuring equipment. The voltages of rows 1, 2, and 3 (1S3P-1 to 3) of 3S3P is represented as V_H, V_M, and V_L, respectively.

3. Experimental Results and Discussions

3.1. VRP of Individual Cells

The OCVs recorded during the 4 h of rest after charging at a different C_{rate} were processed and the VRP was computed. The results from the individual cell tests were analyzed and it was seen that the cell VRPs exhibited lithium stripping only for 0.5 and 1C at ambient temperatures of 5 and 0 °C. The VRPs for these scenarios are depicted in Figure 5. The pointers in the figures show the deflection in VRP, indicating the end of Li stripping.

It can be seen in Figure 5a, for 25 and 10 °C, the Li stripping characteristics are not observed in the OCV, even for a higher Crate of 1C. This is due to improved charge kinetics and diffusion at high temperatures. The two-stage decay in OCV is predominantly seen in the VRP at lower temperatures. All the cells were maintained at the same temperature, and the maximum deviation from the setpoint value was ±0.5 °C. However, cell-to-cell variations were prominent in the result obtained. Cells 1 to 3 exhibited higher, cells 4 to 6 had moderate, and cells 7 to 9 had minimum levels of stripping.

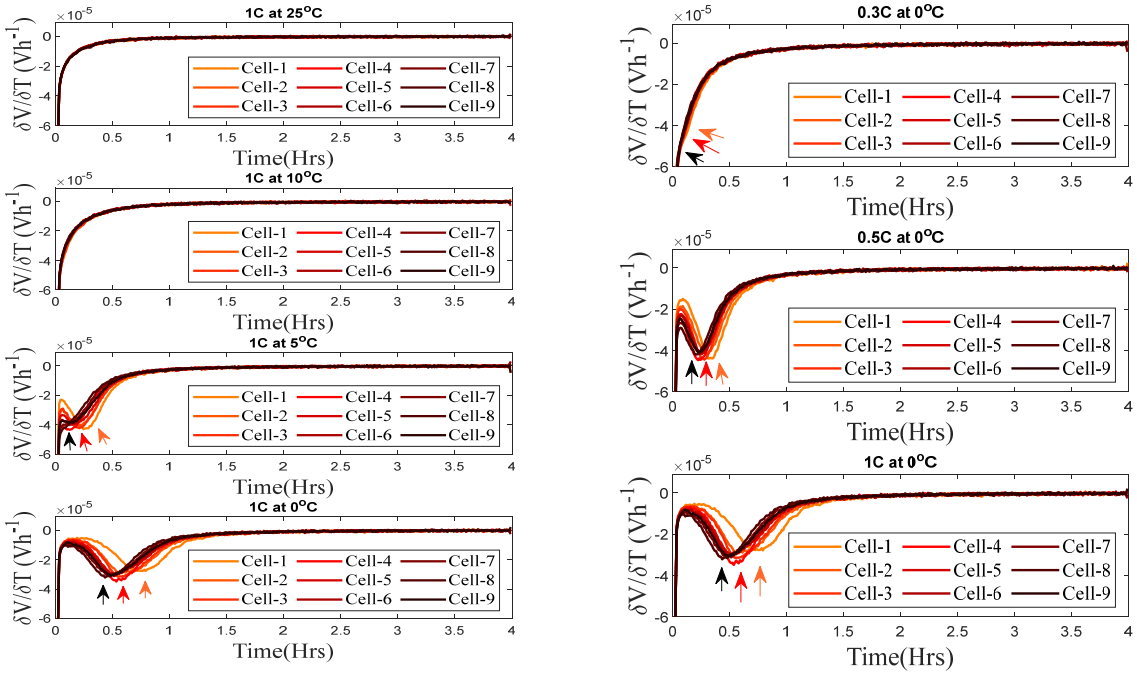

Figure 5. VRP of individual cells. (**a**) Effect of temperature when cells are charged at 1C. (**b**) Effect of C_{rate} when cells are kept at 0 °C.

An ambient temperature of 0 °C stimulated more Li stripping associated with reversible LP for the cells considered, even for lower currents of 0.3C. The influence of C_{rate} on Li stripping at 0 °C is revealed in Figure 5b. From these results, it could be seen that the VRP is only effective in detecting the possible onset of LP for temperatures of 5 °C and below when cells are charged at 0.5 and 1C. Hence, it is possible that the VRP may only be effective for similar scenarios when these cells are connected in series-parallel combination. This is evaluated in the following sections.

3.2. VRP of 1S3P Configuration

The charge and discharge protocols programmed in the Maccor were modified to suit the 1S3P configuration of cells. The charge–discharge currents and CV cut-off limits were scaled up by a factor of three to suit 1S3P cycling. The test scenarios of individual cell tests were repeated on all the 1S3P modules and the VRP was computed from the rest period OCV. In addition, the inter-cell current flow during cycling and relaxation was monitored.

As the cells under consideration showed signs of stripping only for lower temperatures during individual cycling, only those scenarios are repeated for 1S3P configurations. The relaxation OCV of cells in 1S3P connection differed from their individual tests for 5 and 0 °C, as seen in Figure 6. The VRP of modules from relaxation OCV for the same temperatures are shown in Figure 7.

The VRP of 1S3P modules deviated significantly from the individual cell results shown in Figure 5a, especially for 5 °C. The 1S3P's OCVs and corresponding VRPs did not reveal any signs of Li stripping at 5 °C in Figures 6a and 7a. Although stripping was observed for 0 °C, the characteristics are different from the individual cell results seen in Figure 7b. To understand if this varied OCV and VRP behavior is due to unbalanced charging of cells within each 1S3P, charging and relaxation currents at 0 °C are also analyzed.

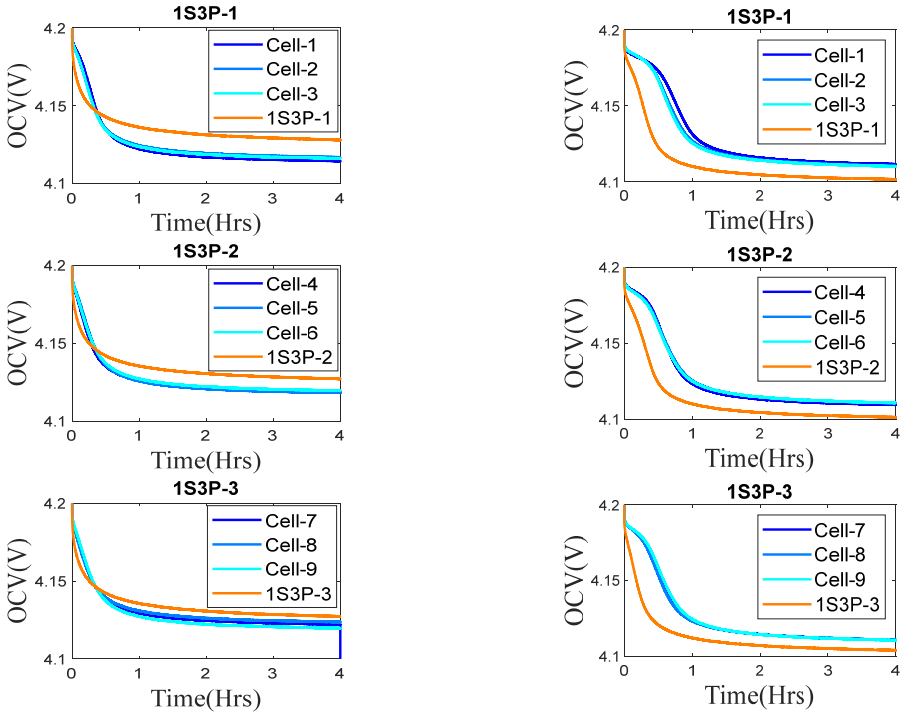

Figure 6. OCV of cells charged at 1C, individually and in 1S3Ps: (**a**) At 5 °C. (**b**) At 0 °C.

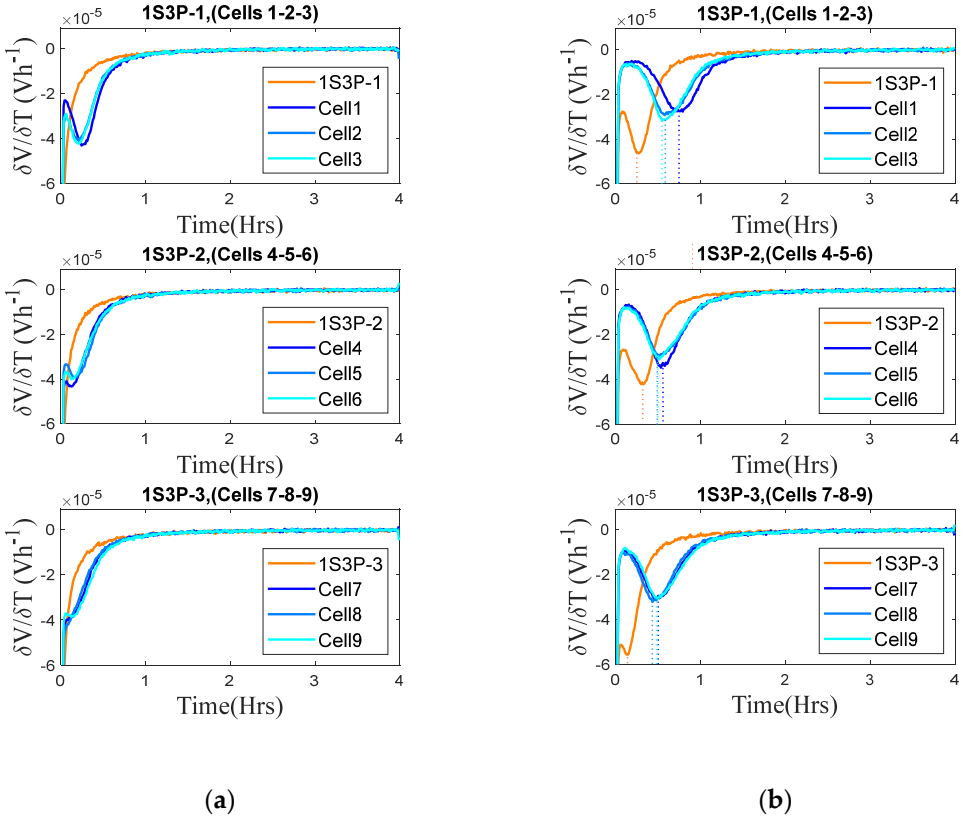

Figure 7. Comparison of VRPs when cells are charged at 1C, individually and in 1S3Ps: (**a**) At 5 °C. (**b**) At 0 °C.

The charging currents recorded by ADC-24 for an ambient temperature of 0 °C charged at 1C were processed and coulomb counting was employed to estimate the SoC based on (1). The ampere hour of each cell, when tested in 1S3P for 0 °C and 1C, is computed. As the energy capacity of each cell for 1C at 0 °C is unknown prior to the 1S3P test, the relative SoC is computed with the capacity from RPT-2 as per Equation (1). C_1S3P is the capacity of cells when charged at 1C in 1S3P at 0 °C. Similarly, C_RPT2 is the cell capacity from RPT-2 performed before the experiment. Though the capacity from RPT is measured at a different temperature and C_{rate}, it is a reliable reference to effectively assess the cells. Table 1 shows the computed values based on (2).

$$SoC(t) = SoC(t-1) + \frac{\Delta t \times i(t)}{3600 \times Cell\_capacity} \quad (1)$$

$$SoC\_1S3P_{Relative} = \left(C\_1S3P/C\_RPT2\right) \times 100 \quad (2)$$

Table 1. Relative SoC of cells in 1S3Ps after 1C charging at 0 °C.

Module	**1S3P 1**			**1S3P 2**			**1S3P 3**		
Cells	cell1	cell2	cell3	cell4	cell5	cell6	cell7	cell8	cell9
$SoC\_1S3P_{Relative}$ (%)	90.68	92.68	88.19	90.80	91.14	90.23	91.25	92.28	90.53

The average of cell capacities from RPT-2 was 4.39 Ah, with a standard deviation of 0.17 Ah. From the $SoC\_1S3P_{Relative}$(%) it is implied that the cells in 1S3Ps are balanced, especially in 1S3P-2 and 3. The variations seen in 1S3P-1 cells may primarily be due to the parasitic resistances from jig fixtures and brass blocks at lower temperatures.

The analysis of rest phase currents showed an interesting relationship with the OCV during rest. Ideally, stripping of metallic lithium and the re-intercalation into the anode will cause a voltage plateau that can be clearly seen in the OCV of an individual cell. When the cells are connected in parallel as part of a module, they are not in open circuit and the voltage plateau of an individual cell will cause current flow within the module. The correlation of current flow and voltage plateau was significant for 0 °C. During the 5 °C rest period in Figure 8a, the current flow seems to be steady, without dynamic changes. The initial current flow between cells was noticed to be influenced by the voltage plateau, as seen in Figure 8b. The start and end of the voltage plateau in OCV is indicated by red arrowheads. Positive and negative currents indicate cells charging and discharging, respectively. Only the significant first 1 h of the current flow is shown here.

The steady current flow during rest seems to affect the Li stripping process, and hence, the voltage plateau is negligible at 5 °C and not captured in the VRP. However, as seen during individual cell tests, stripping is prevalent at 0 °C and this explains the plateau in Figure 8b. Stripping is initiated within each cell in 1S3Ps, there will be variations in the plateaus of the individual cells, as observed in Figure 5a in Section 3.1. Nevertheless, since cells are connected in parallel, they cannot have different voltages and this leads to counteracting current flow within each 1S3P branch. Once stripping is completed, the dynamics in current flow settles down and steady balancing current flow continues to exist till the end of 4 h rest.

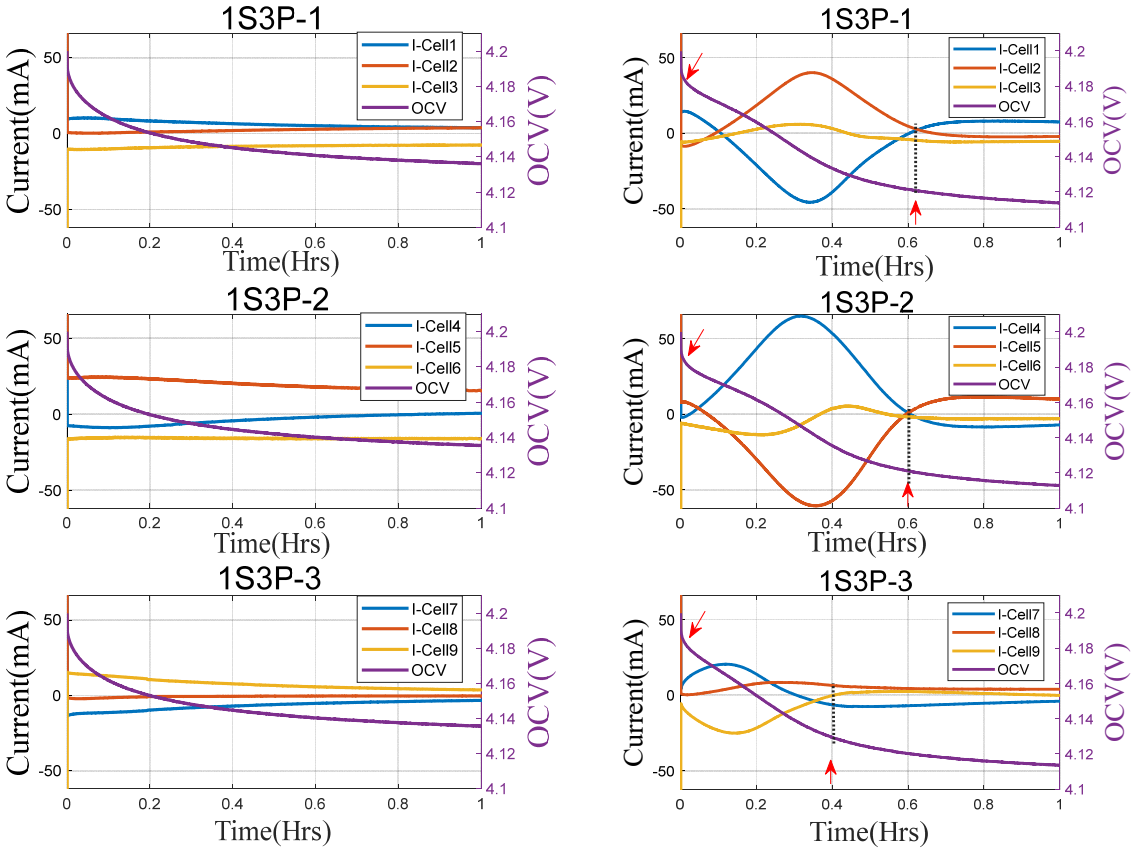

(**a**) (**b**)

Figure 8. OCV and rest phase currents after 1C charge: (**a**) At 5 °C. (**b**) At 0 °C.

3.3. VRP of 3S3P Configuration

The experiments on individual cells were repeated for 3S3P, with the Chroma module cycler programmed appropriately with revised charge/discharge limits. The controller area network (CAN) messages from the BMS were used as limits for the cycler in real time. The highest cell voltage measured by BMS was used as the limit for CC charging. Similarly, the lowest cell voltage data from BMS was set as the limit during CC discharge. This is to avoid over charging and over discharging.

The VRP of each 1S3P in the module was computed from the respective ISO224 voltage sensor data. In addition to this, the VRP of 3S3P was computed from the module OCV data recorded by the Chroma cycler.

The results from 3S3P testing showed Li stripping only for 0 °C with 1C charging, as noticed in 1S3P testing (Section 3.2). The VRPs of the 3S3P module and 1S3Ps within the module are depicted in Figure 9. Rows 1, 2, and 3 represent 1S3P-1, 2, and 3, respectively.

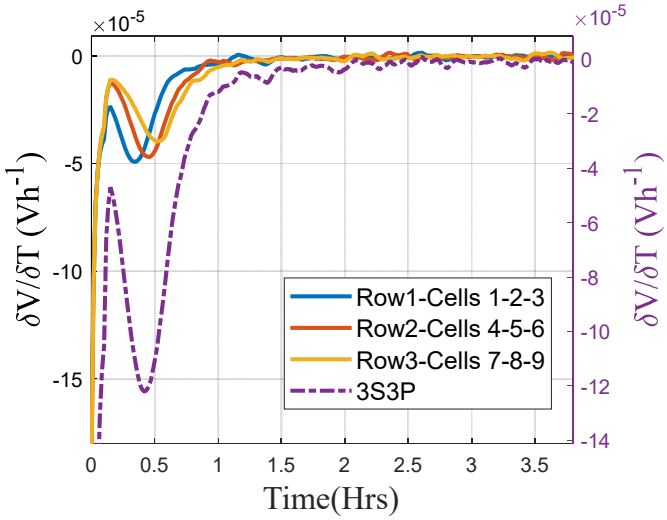

Figure 9. VRPs from 3S3P module.

In Figure 9, the VRP of the 3S3P module is an algebraic sum of individual 1S3P VRPs. Hence, it is important to compute the VRP of each row of a bigger module, as there could be varied levels of LP and the VRP computed from net module OCV need not reflect this. This is crucial when performance of FC strategies are monitored based on VRP as detailed in [9]. The stripping time for row 3 (1S3P-3) is seen to be slightly more than rows 2 and 1, indicating varied levels of LP within the module.

The stripping times measured from Figure 9 are given in Table 2. Compared with row 1, the stripping time for rows 2 and 3 were 1.36 and 1.6 times higher, respectively. The VRP of 3S3P computed from the module OCV showed a stripping time of 24.6 min, which is 1.3 times less than row 3. This clearly shows the significance of computing row wise VRPs, rather than one from module OCV. To investigate the varied levels of plating within 3S3P, the surface temperature and charging current of each cell are analyzed and given in Figure 10.

Table 2. Stripping time from VRPs of 3S3P.

Module Name	Details	Stripping Time (Min)
1S3P-1	OCV from ISO224 (V_H)	19.8
1S3P-2	OCV from ISO224 (V_M)	27
1S3P-3	OCV from ISO224 (V_L)	31.8
3S3P	Module OCV from cycler	24.6

Current and temperature variation during the CC phase is focused on here. A temperature gradient of 1 °C is observed within the module before 1C charging; this may be due to non-uniform circulation within the chamber. Cells in 1S3P-2 and 3 were at a lower temperature (<0 °C) than 1S3P-1. Furthermore, during charging the rise in temperature (ΔT) is small for 1S3P-3. The dependence of LP on temperature [19,20] favored more LP, and this resulted in the extended stripping time in Table 2. In the case of 1S3P-2, though the cells were initially at lower temperature, during charging the ΔT increased.

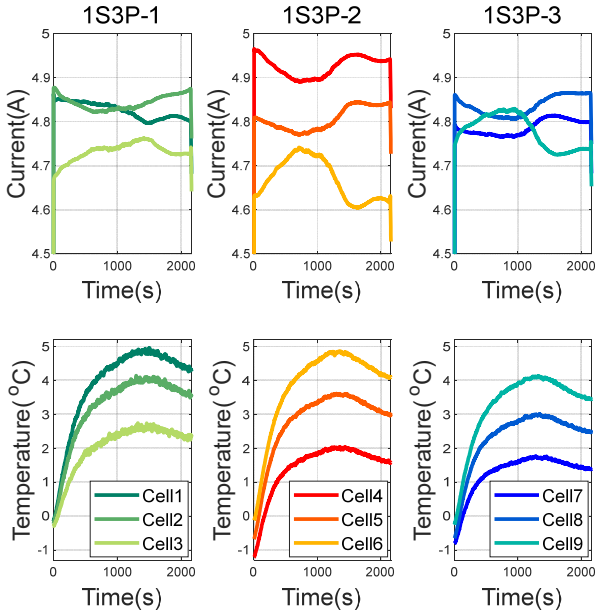

Figure 10. Charging current and surface temperature of cells in 3S3P, 1C at 0 °C.

The relative SoC of each cell in 3S3P is computed based on RPT-3 as per Equation (3) and given in Table 3.

$$SoC\_3S3P_{Relative}(\%) = (C\_3S3P/C\_RPT3) \times 100 \quad (3)$$

Table 3. Relative SoC of cells in 3S3P after 1C charging at 0 °C.

Module	**1S3P 1**			**1S3P 2**			**1S3P 3**		
Cells	cell1	cell2	cell3	cell4	cell5	cell6	cell7	cell8	cell9
$SoC\_3S3P_{Relative}(\%)$	85.07	86.43	84.07	89.03	85.16	81.97	84.71	86.39	83.94

The $SoC\_3S3P_{Relative}$ data in Table 3 suggest cell unbalance in 3S3P. Yet, the average of cell SoCs within each row of 3S3P is 85.19, 85.38, and 85.01%. Similarly, the standard deviation of cell SoCs in each row is 1.18, 3.53, and 1.25%. Cells in 1S3P-1 and 3 are relatively balanced compared with 1S3P-2. During charging, the voltage of 1S3P-3 reached the CC limit (4.2 V). First, this was sensed by the BMS, and subsequently, the cycler changed from CC to CV mode.

The 1S3P-1 and 3 were at a lower voltage and later at a CV limit of 0.15C charging stopped. This led to the unbalance in cell SoCs at lower ambient temperatures. Also, the variations in the test jig connections and parasitic resistances changes the current flow within module. Although care has been taken to minimize the error in measurements, minor errors in current measurement can affect the computations based on KCL and, when aggregated during coulomb counting, can lead to variations in cell SoCs.

The rest phase current after charging was comparable with the results from the 1S3P experiment as seen in Figure 8b. The dynamics in current flow and OCV were correlated, and after stripping the currents stabilized and continued to flow till the end of the 4 h rest. The dynamics in current and OCV during relaxation are depicted in Figure 11.

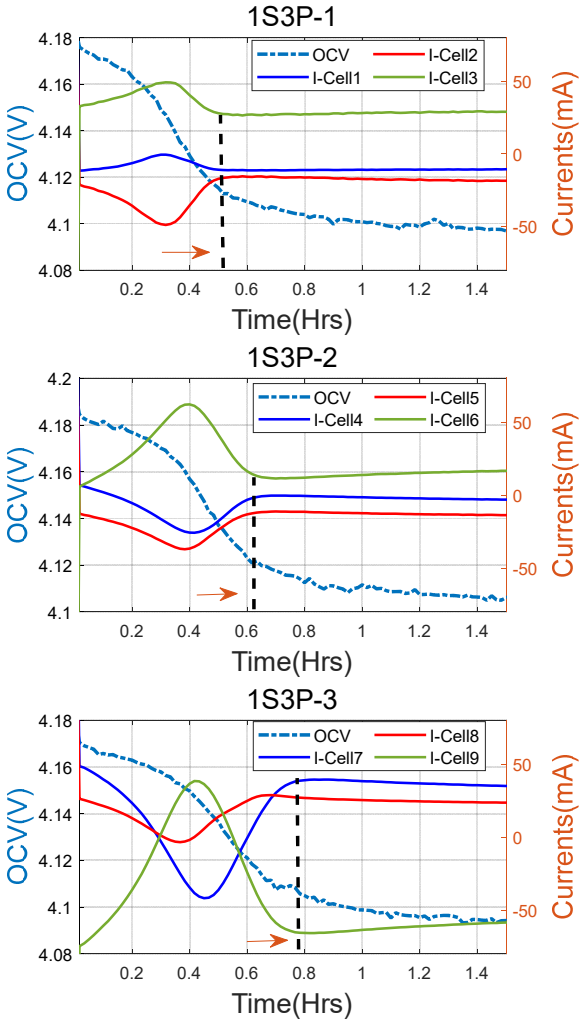

Figure 11. OCV and rest phase currents in 3S3P after 1C charge at 0 °C.

The rest period current flow in 1S3P-3 in Figure 11 was significantly higher than when the same cells were tested as an independent 1S3P in Figure 8b. The cells in 1S3P-3, when tested individually, showed lower stripping time, as seen in Figure 5. These cell variations can induce varied levels of LP for cells within 1S3P-3 and lead to distinct rest phase currents. The arrowhead in Figure 11 specifies the end of the dynamics in current and relates to the end of the voltage plateau. The cells in 1S3P-3 were charged to similar SoCs, with a deviation of only 1.25% from the mean, yet the current flow during the rest phase is prevalent. As these cells experienced varied levels of plating, the voltage plateau of each during rest may have been distinct, and this led to the dynamics in current flow, as the parallel connection forces cell voltages to be same.

4. Future Works

4.1. Evaluation on Different Cell Chemistries

The study conducted here focused on cells with NCA as the cathode material. Though the VRP should ideally work for any cells with graphite anode, it is to be studied in detail for other cell chemistries and material ratios. The comparison of the relaxation behavior of different chemistries is not yet studied and compared. Another important aspect to consider is the influence of differently aged cells within a module.

4.2. Module Formats, Representative Bus Bars, and Interconnections

The results from testing individual 1S3Ps and when they were in series to form 3S3P showed variations in charging currents and lithium stripping. This clearly suggests the dependence of LP and anode potential on module formats and interconnections. The efficacy of the VRP for lithium stripping detection when more cells are connected in series-parallel are to be investigated and substantiated.

The scale-up performed for the study utilized generic jigs to facilitate additional current and voltage measurements, and the effect of parasitic circuit parameters were noticeable. A battery module with actual bus bars, interconnections, and with multi sensor array boards for measurements discussed in [16] can drastically reduce these and aid in future assessments.

One of the main challenges is to have accurate current measurements during cycling and during rest. The sensors utilized should be capable of measuring current in the range of milliamperes during rest and measure large currents up to 1C. A single sensor might not be feasible for this. Hence, a combination of sensors with different ranges could be utilized. The sensitivity and accuracy of voltage measurement is equally important, as the whole VRP analysis depends on it.

4.3. Temperature Gradient within the Pack

It is evident from the experiment results and existing literature that LP is highly influenced by temperature. The study here focused on cells/modules kept in an environmental chamber and ambient temperature was maintained constant as much as possible. Temperature gradients in a battery pack could be due to unbalanced charging or even due to ineffective cooling mechanisms. Cells tend to degrade within a parallel system due to uneven current distribution [21], and the temperature gradient [22] is a prime factor for this. As considered by Zilberman et al., a much larger temperature gradient could be induced within a small module in a controlled environment and the occurrence of voltage plateau and stripping could be studied.

5. Conclusions

The study presented here focused on assessing the ability of the VRP to detect LP for cells and cells in series-parallel connections. The test conditions considered various charging scenarios and temperatures, with current flow measurements within the battery modules. It was found that the VRP detects lithium stripping associated with LP even if cells are not ideally in open circuit. The transferability of the VRP from individual cells to modules proved to be feasible. However, the detection capability and sensitivity of the VRP at the module level was severely reduced in comparison to single cell tests. Low levels of LP did not show any plateaus in the OCV during rest. The promising results obtained from the study were limited to lower temperatures and a high C_{rate}, both are known to cause severe plating. This result implies that BMS algorithms designed and calibrated within a laboratory using single cell experiments will need to be recalibrated for deployment on multicell systems relative to the actual architecture of the battery pack employed.

FC strategies usually incorporate C_{rates} well above 1C and gradually reduce based on SoC and temperature during charging. Hence, for such studies the VRP will be useful, particularly for temperatures lower than 5 °C. The VRP could be scaled and used within a BMS as a tool to detect LP. Yet, the role of it in a BMS is limited and it can only act as a binary indicator of LP. As seen from the results, analyzing a single voltage plateau from module OCV may lead to inaccurate estimation of LP. It is highly recommended to consider OCVs of each series branch to distinguish variations within the module. These voltages are normally measured by BMS to find the highest and lowest cell voltages in a pack.

For high temperatures and a lower C_{rate}, the VRP failed to provide necessary insights and the incidence of LP could be misinterpreted. The VRP of single cells and cells in parallel for the study in [17] were comparable. However, the experimental results presented here disagree with the findings. One reason for this is the calendar ageing of cells; cells from

different manufacturing batches tend to be aged differently. Furthermore, the cathode and anode thickness also play a vital role in LP. Small deviations in these can lead to different stripping behavior and VRPs. The detection capability of the VRP is known to improve when cut-off current in the CV phase is adjusted appropriately. The influence of this on cells in series-parallel connection is a topic that needs to be researched.

Author Contributions: Conceptualization, N.S., N.F.S. and J.M.; methodology, N.S. and N.F.S.; validation, N.S.; formal analysis, N.S.; investigation, N.S. and N.F.S.; resources, J.M.; data curation, N.S.; writing—original draft preparation, N.S. and N.F.S.; writing—review and editing, J.M. and T.Q.D.; supervision, J.M. and T.Q.D. All authors have read and agreed to the published version of the manuscript.

Funding: This research is supported by Innovate UK through the Electric BSA (eBSA), Project Number: 75281.

Data Availability Statement: The data presented in this study are available on request from the corresponding author.

Acknowledgments: The authors record their sincere gratitude to James Mathew, project engineer at WMG, for his contributions during module testing.

Conflicts of Interest: The authors declare no conflict of interest.

Abbreviations

LP	Lithium plating
FC	Fast charging
VRP	Voltage relaxation profile
CC	Constant current
CV	Constant Voltage
Crate	Charging rate
OCV	Open-circuit voltage
RPT	Reference performance test
1S3P	1 cell in series and 3 in parallel
3S3P	3 cells in series and 3 in parallel
BMS	Battery management system

References

1. Shahriar, S.; Al-Ali, A.R.; Osman, A.H.; Dhou, S.; Nijim, M. Machine learning approaches for EV charging behavior: A review. *IEEE Access* **2020**, *8*, 168980–168993. [CrossRef]
2. Bose, B.; Garg, A.; Panigrahi, B.K.; Kim, J. Study on Li-ion battery fast charging strategies: Review, challenges and proposed charging framework. *J. Energy Storage* **2022**, *55*, 105507. [CrossRef]
3. Gupta, C.; Das, M. Multiphase Interleaved DC-DC Converter for Fast Charging Application of Electric Vehicles. In Proceedings of the 2022 IEEE 16th International Conference on Compatibility, Power Electronics, and Power Engineering (CPE-POWERENG), Birmingham, UK, 29 June–1 July 2022. [CrossRef]
4. Lin, X.; Khosravinia, K.; Hu, X.; Li, J.; Lu, W. Lithium Plating Mechanism, Detection, and Mitigation in Lithium-Ion Batteries. *Prog. Energy Combust. Sci.* **2021**, *87*, 100953. [CrossRef]
5. Wang, H.; Zhu, Y.; Kim, S.C.; Pei, A.; Li, Y.; Boyle, D.T.; Wang, H.; Zhang, Z.; Ye, Y.; Huang, W.; et al. Underpotential lithium plating on graphite anodes caused by temperature heterogeneity. *Proc. Natl. Acad. Sci. USA* **2020**, *117*, 29453–29461. [CrossRef] [PubMed]
6. Chen, Y.; Torres-Castro, L.; Chen, K.H.; Penley, D.; Lamb, J.; Karulkar, M.; Dasgupta, N.P. Operando detection of Li plating during fast charging of Li-ion batteries using incremental capacity analysis. *J. Power Sources* **2022**, *539*, 231601. [CrossRef]
7. Waldmann, T.; Kasper, M.; Wohlfahrt-Mehrens, M. Optimization of Charging Strategy by Prevention of Lithium Deposition on Anodes in high-energy Lithium-ion Batteries-Electrochemical Experiments. *Electrochim. Acta* **2015**, *178*, 525–532. [CrossRef]
8. O'Kane, S.E.J.; Campbell, I.D.; Marzook, M.W.J.; Offer, G.J.; Marinescu, M. Physical Origin of the Differential Voltage Minimum Associated with Lithium Plating in Li-Ion Batteries. *J. Electrochem. Soc.* **2020**, *167*, 090540. [CrossRef]
9. Konz, Z.M.; Konz, Z.M.; McShane, E.J.; McShane, E.J.; McCloskey, B.D.; McCloskey, B.D. Detecting the Onset of Lithium Plating and Monitoring Fast Charging Performance with Voltage Relaxation. *ACS Energy Lett.* **2020**, *5*, 1750–1757. [CrossRef]
10. Koleti, U.R.; Zhang, C.; Dinh, T.Q.; Marco, J.; Amietszajew, T.; Malik, R. A new concept to improve the lithium plating detection sensitivity in lithium-ion batteries. *Int. J. Smart Grid Clean Energy* **2019**, *8*, 505–516. [CrossRef]

11. Campbell, I.D.; Marzook, M.; Marinescu, M.; Offer, G.J. How Observable Is Lithium Plating? Differential Voltage Analysis to Identify and Quantify Lithium Plating Following Fast Charging of Cold Lithium-Ion Batteries. *J. Electrochem. Soc.* **2019**, *166*, A725–A739. [CrossRef]
12. Janakiraman, U.; Garrick, T.R.; Fortier, M.E. Review—Lithium Plating Detection Methods in Li-Ion Batteries. *J. Electrochem. Soc.* **2020**, *167*, 160552. [CrossRef]
13. Koleti, U.R.; Dinh, T.Q.; Marco, J. A new on-line method for lithium plating detection in lithium-ion batteries. *J. Power Sources* **2020**, *451*, 227798. [CrossRef]
14. Koleti, U.R.; Bui, T.N.M.; Dinh, T.Q.; Marco, J. The Development of Optimal Charging Protocols for Lithium-Ion Batteries to Reduce Lithium Plating. *J. Energy Storage* **2021**, *39*, 102573. [CrossRef]
15. Koseoglou, M.; Tsioumas, E.; Ferentinou, D.; Jabbour, N.; Papagiannis, D.; Mademlis, C. Lithium plating detection using dynamic electrochemical impedance spectroscopy in lithium-ion batteries. *J. Power Sources* **2021**, *512*, 230508. [CrossRef]
16. Luca, R.; Whiteley, M.; Neville, T.; Tranter, T.; Weaving, J.; Marco, J.; Shearing, P.R.; Brett, D.J. Current Imbalance in Parallel Battery Strings Measured Using a Hall-Effect Sensor Array. *Energy Technol.* **2021**, *9*, 202001014. [CrossRef]
17. Somasundaran, N.; Saniee, N.F.; Quang, T.D.; Marco, J. Feasibility Assessment of Differential Voltage Analysis to Detect Lithium Plating in Battery Modules for Electric Vehicles. In Proceedings of the 25th International Conference on Mechatronics Technology (ICMT), Wuhan, China, 28–29 October 2022; pp. 1–6. [CrossRef]
18. Gulsoy, B.; Vincent, T.A.; Sansom, J.E.H.; Marco, J. In-situ temperature monitoring of a lithium-ion battery using an embedded thermocouple for smart battery applications. *J. Energy Storage* **2022**, *54*, 105260. [CrossRef]
19. Cabañero, M.A.; Altmann, J.; Gold, L.; Boaretto, N.; Müller, J.; Hein, S.; Zausch, J.; Kallo, J.; Latz, A. Investigation of the temperature dependence of lithium plating onset conditions in commercial Li-ion batteries. *Energy* **2019**, *171*, 1217–1228. [CrossRef]
20. Saniee, N.F.; Somasundaran, N.; Gulsoy, B.; Vincent, T.; Amor-Segan, M.; Marco, J. Analysis of Internal Temperature Variations of Lithium-Ion Batteries During Fast Charging. In Proceedings of the 25th International Conference on Mechatronics Technology (ICMT), Wuhan, China, 28–29 October 2022; pp. 1–5. [CrossRef]
21. Klein, M.P.; Park, J.W. Current Distribution Measurements in Parallel-Connected Lithium-Ion Cylindrical Cells under Non-Uniform Temperature Conditions. *J. Electrochem. Soc.* **2017**, *164*, A1893–A1906. [CrossRef]
22. Zilberman, I.; Ludwig, S.; Schiller, M.; Jossen, A. Online aging determination in lithium-ion battery module with forced temperature gradient. *J. Energy Storage* **2020**, *28*, 101170. [CrossRef]